Bi-modular fusion proteins, a versatile therapeutic tool for re-directing a pre-existing Epstein-Barr virus antibody response towards defined target cells

Benoît Gamain
INSERM https://orcid.org/0000-0002-8255-2145
Carine Brousse
INSERM
Nathan Rainey
INSERM
Béré Diallo
INSERM
Clara-Eva Paquereau
INSERM
Alexandra Desrames
INSERM
Jolita Ceputyte
INSERM
Jean-Philippe Semblat
Institut National de la Transfusion Sanguine
Olivier Bertrand
INSERM
Stéphane Gangnard
INSERM
Jean-Luc Teillaud
INSERM https://orcid.org/0000-0003-4442-9565
Arnaud CHENE (arnaud.chene@inserm.fr)
INSERM

Article

Keywords: Epstein-Barr virus, polyclonal antibody response, bi-modular fusion proteins

Posted Date: June 29th, 2021

DOI: https://doi.org/10.21203/rs.3.rs-668626/v1

Bi-modular fusion proteins, a versatile therapeutic tool for re-directing a pre-existing Epstein-Barr virus antibody response towards defined target cells

Benoît Gamain[1], Carine Brousse[1], Nathan Rainey[1], Béré K. Diallo[2], Clara-Eva Paquereau[1], Alexandra Desrames[1], Jolita Ceputyte[1], Jean-Philippe Semblat[1], Olivier Bertrand[1], Stéphane Gangnard[1], Jean-Luc Teillaud[2], Arnaud Chêne[1,*]

[1] Université de Paris, Biologie Intégrée du Globule Rouge, UMR_S1134, Inserm, F-75015, Paris, France.

[2] Laboratory « Immune Microenvironment and Immunotherapy », Inserm U.1135, Centre d'immunologie et des maladies infectieuses (CIMI-Paris), Faculté de médecine, Sorbonne Université, 91 boulevard de l'hôpital, 75013, Paris, France.

Running Title: Redirecting anti-EBV antibodies to the surface of target cells

[*]**Correspondence:**

Arnaud Chêne

INSERM (UMR_S1134)

6 rue Alexandre Cabanel, 75015 Paris, France

Phone : 0033 (0) 1 44 49 31 08

E-mail : arnaud.chene@inserm.fr

ABSTRACT

Industrial production of therapeutic monoclonal antibodies is mostly performed in eukaryotic-based systems, allowing post-translational modifications mandatory for their functional activity. Nevertheless, the resulting elevated product cost limits therapy access to some patients, thus increasing medical inequality. To address this limitation, we conceptualized a novel immunotherapeutic approach aiming at redirecting a pre-existing polyclonal antibody response against Epstein-Barr virus (EBV) towards defined target cells. We engineered bi-modular fusion proteins (BMFPs), notably expressible in bacteria-based systems, comprising a Fc-deficient binding moiety (Nanobody, scFv) specifically targeting an antigen expressed at the surface of a target cell, fused to the P18 EBV antigen, which would recruit circulating endogenous anti-P18 IgG in individuals chronically infected by EBV. Opsonization of BMFP-coated target cells efficiently triggered antibody-mediated clearing effector mechanisms *in vitro,* such as the complement cascade, erythrophagocytosis by macrophages and FcγRIII-mediated activation of cellular pathways leading to antibody-dependent cell-mediated cytotoxicity (ADCC). When assessed in a mouse tumour model, therapy performed with an anti-huCD20 BMFP significantly led to increased mice survival and total cancer remission in some animals. These results indicate that BMFPs are versatile tools for redirecting an Epstein-Barr virus pre-existing immune antibody response towards pre-defined target cells and could represent potent and useful therapeutic molecules to treat a broad range of diseases.

MAIN

The generation of therapeutic monoclonal antibodies (mAbs) is a tedious process, which requires integrating the complex structural and biochemical features of the immunoglobulin (Ig) molecules to achieve the desired effector functions and exhibit optimal *in vivo* efficacy[1,2]. Over the past decades, mAbs developed to deplete target cells such as tumour cells or normal auto-immune cells, for instance B cells in multiple sclerosis, have drawn a particular attention and significant efforts have been undertaken to engineer Igs with optimized biological activity and improved pharmacokinetic (PK) properties[3,4]. Fragment crystallizable (Fc)-mutated and glyco-engineered IgG have been developed to maximize their potential to trigger complement-dependent cytotoxicity (CDC)[5,6], antibody-dependent cell-mediated cytotoxicity (ADCC)[7,8,9,10] and antibody-dependent phagocytosis (ADP)[11]. Engineering of the Fc region of IgG have also permitted to modulate the pH-dependent affinity of some antibodies for neonate Fc receptors (FcRn), consequently modifying the mAb PK properties and enhancing *in vivo* half-life[12,13].

The vast majority of mAbs are repeatedly injected at high doses to achieve significant therapeutic effects[14]. MAb production has therefore to be achieved at very large scale. Today, most therapeutic mAbs are expressed in eukaryotic cell-based systems, allowing the production of large quantities of functional proteins presenting proper post-translational modifications such as glycosylation. However, such systems require arduous selection processes and long production cycles resulting in increased mAb manufacturing cost. Thus, the development of mAb-based therapies present substantial hurdles and remains challenging in particular when long-term iterative treatments are needed.

Thus, we envisioned the possibility of generating bi-modular fusion proteins (BMFPs) able to redirect polyclonal endogenous high-affinity antibodies produced by memory B cells against

Epstein-Barr virus (EBV) towards defined target cells. BMFPs could then be designed based on an EBV antigen coupled to a specific ligand targeting a protein of interest on the surface of a target cell. BMFPs could circumvent the need for all the complex engineering studies aiming at improving the effector functions of a single monoclonal antibody and also allow the use of diverse ligand units devoid of Fc chains, such as nanobodies, to trigger Fcγ-dependant antibody effector mechanisms by recruiting anti-EBV polyclonal antibodies exhibiting a large spectrum of functions and produced over long periods of time in individuals. Expressible in bacteria-based systems, BMFPs could be produced at a low manufacturing cost as compared to current therapeutic mAbs, offering broader access to patients.

EBV is a ubiquitous human herpes virus (HHV-4) that infects over 95% of the adult population worldwide[15]. Following primary infection, EBV establishes a life-long persistent infection, residing in a latent stage in memory B cells[16]. The persistence of the virus results from a fine balance between viral latency, viral replication and host immune responses[17]. As a consequence, infected individuals possess, all along their life, antibodies directed against various EBV antigens including the conserved small capsomere-interacting protein P18 (ORF BFRF3) (**Supplementary Fig. 1**), which is predominantly recognized by antibodies belonging to the IgG1 subclass[18]. This human IgG subclass is the most commonly used for therapeutic antibodies, whatever their formats (chimeric, humanized or fully human mAbs)[19], as it triggers and regulates effector immune mechanisms via the binding of the Fcγ region to the complement component C1q[20,21] and to Fcγ receptors (FcγRs) present at the surface of a broad range of leukocytes sub-populations[22,23]. It also triggers pro-inflammatory or anti-inflammatory processes depending on the sialylation on the N-linked glycan of the Fc region[24]. Thus, a P18-containing fusion molecule with a predefined binding specificity could allow the recruitment of endogenous anti-P18 IgG1 antibodies at the surface of

target cells and then trigger Fc-dependent and complement-dependent immune effector mechanisms (**Fig. 1**).

As a proof of concept, we generated different sets of BMFPs comprising P18-derived antigens fused to i) a nanobody (Nb) directed against the Duffy Antigen Receptor for Chemokines (DARC) expressed by mature red blood cells (RBCs) (**Fig. 1 – model 1**) and ii) a single-chain variable fragment (scFv) directed against the human cluster of differentiation huCD20 expressed on most mature B cells, which represents an exquisite target for antibody-based therapy of B cell-related diseases (**Fig. 1 – model 2**). Following extensive biochemical characterisation, the ability of these BMFPs to trigger target cell depletion through the recruitment of pre-existing anti-P18 antibodies was assessed in various *in vitro* assays. An *in vivo* mouse tumour model, previously developed to explore the vaccinal effect of anti-tumor antibodies[25,26], was also used to evaluate the anti-tumor capacity of anti-huCD20 BMFPs (**Fig. 1 – model 2)** injected into mice possessing anti-P18 antibodies.

We show herein that functional BMFPs against human RBCs and huCD20$^+$ cells bind efficiently to their respective cellular targets and recruit anti-P18 antibodies at the cell surface, triggering efficient immune effector functions. A strong *in vitro* RBC phagocytosis by macrophage-like cells derived from FcγRI$^+$/RIIa$^+$ monocytic leukemia THP1 cells was detected when using anti-DARC BMFPs in combination with IgG present in the plasma of EBV$^+$ individuals. We also show that *in vitro* treatment of huCD20$^+$ Burkitt's lymphoma cells with an anti-huCD20 BMFP elicits a significant activation of the antibody-dependent complement cascade and triggers a FcγRIII-mediated activation of the nuclear factor of activated T cells (NFAT) pathway in an ADCC reporter assay in presence of plasma containing anti-P18 antibodies. Finally,

we show an increased survival of P18-pre-immunized immunocompetent mice bearing huCD20^{+} tumor cells following anti-huCD20 BMFP treatment.

All together, these results indicate that BMFPs are versatile tools for redirecting a pre-existing Epstein-Barr virus immune antibody response towards pre-defined target cells and could represent potent and useful therapeutic molecules in patients.

RESULTS

Engineering bi-modular fusion proteins (BMFPs) against DARC.

DARC, also known as Fy glycoprotein, is a promiscuous chemokine receptor abundantly present at the surface of RBCs from individuals carrying the FY^{a+}/FY^{b+}, FY^{a-}/FY^{b+} or FY^{a+}/FY^{b-} genotypes[27] and was therefore considered as a molecular target of choice to generate a first set of BMFPs targeting human erythrocytes in a proof of concept model (**Fig. 1 – model 1)**. To generate anti-DARC BMFPs, we chose a nanobody targeting the extracellular domain 1 (ECD1), which specifically binds to DARC^{+} human RBCs with high affinity[28]. The CA52 anti-DARC nanobody (Nb-αDARC) was genetically fused to the N-terminus part of full-length P18 (P18FL) or of P18 fragments of different sizes (P18F2, P18F3, P18F4) **(Fig. 2a, b).** The resulting recombinant constructs were expressed in *E. coli* SHuffle bacteria, which allow disulfide bond formation within the cytoplasm[29] (see the BMFP production scheme in **Supplementary Fig. 2)**. Soluble non-aggregated Nb-αDARC-P18F2, Nb-αDARC-P18F3, Nb-αDARC-P18F4 and Nb-αDARC could be purified (>95%) in large amounts by size exclusion chromatography (**Fig. 2 c, d**) and used for subsequent experiments. In contrast, the protein solubility of Nb-αDARC-P18FL was poor and led to extensive aggregation during purification, preventing its further use (**Fig. 2c**).

The biochemical and functional properties of Nb-αDARC and P18-derived polypeptides were then sequentially examined. Nb-αDARC, Nb-αDARC-P18F2, Nb-αDARC-P18F3, Nb-αDARC-P18F4 were first subjected to surface plasmon resonance (SPR) analysis to determine their affinity constants for their cognate molecular target, DARC. The extracellular domain of DARC (DARC-ECD1) and the CA52 epitope-mutated form of this domain (DARC-ECD1-Mut), which is no longer recognized by the anti-DARC nanobody (**Supplementary Fig. 3)**, were expressed in *E. coli* as fusion proteins with GST, purified (**Fig. 2e**) and then immobilized on the reference and analytical channels (Fc1 and Fc2, respectively) of a CM5 chip. Sensorgrams are shown in **Figure 2f**. The fitted kinetic data derived from the sensorgrams revealed that the fusion of P18-derived polypeptides to Nb-αDARC did not modify the affinity (K_D constants ranging from 2.75 E^{-11} M to 7.42 E^{-11} M) of the Nb binding moiety for its target as compared to Nb-αDARC alone (K_D=9.00 E^{-11} M) (**Fig. 2f).** Of note, the values of the K_{off} and K_{on} constants of Nb-αDARC-P18F2 markedly differed from those of the two other BMFPs and of Nb-αDARC as shown by a lack of clusterization around Nb-αDARC in the RaPID plot shown in **Fig. 2g**.

The capacity of the BMFPs to be bound by IgG present in the plasma of EBV^+ individuals was then assessed. P18FL, that serves as a reference for IgG binding, was expressed in *E. coli* as a maltose binding protein fusion (MBP-P18FL) to ensure appropriate solubility (**Fig. 2h – left panel**). Enzyme-linked immunosorbent assay (ELISA) performed with 22 individual plasma samples revealed that the binding of circulating IgG to Nb-αDARC-P18F2 and Nb-αDARC-P18F3 were similar to the full-length P18, whereas binding to Nb-αDARC-P18F4 was much lower (**Fig. 2h – right panel**). No binding to Nb-αDARC or to MBP was observed.

Overall, these results positioned P18F3 fused to the Nb-αDARC binding moiety as the shortest P18-derived polypeptide bound by anti-P18 IgG to the same extent as the full-length P18, with no

significant change in the specificity and affinity of the Nb-αDARC part of this BMFP for its cognate target. Nb-αDARC-P18F3 was therefore selected for further functional investigations.

Nb-αDARC-P18F3 binds to native DARC and recruits endogenous anti-EBV IgG to the RBC surface.

The interaction of IgG present in human plasma pools, presenting different recognition levels for the EBV-derived antigen P18F3, with Nb-αDARC-P18F3 bound to native DARC expressed at the surface of $DARC^+$ RBCs (former genotype FY^{a+}/FY^{b+}) was then assessed by flow cytometry (**Fig. 3**). An indirect anti-His-tag fluorescence assay showed first that the fusion of the P18F3 peptide to the C-terminus part of the Nb-αDARC did not prevent the resulting BMFP from binding to RBCs, although a higher concentration was needed to reach the binding plateau as compared to Nb-αDARC (**Supplementary Fig. 4**). Remarkably, in the presence of human plasma pools exhibiting low, intermediate, and high antibody titers against P18F3, the binding of Nb-αDARC-P18F3 to $DARC^+$ RBCs led to the recruitment of anti-P18 IgG and hence to opsonization of the target cells (**Fig. 3a and Supplementary Fig. 5**). The binding amplitude of IgG was in line with the anti-P18F3 antibody titers found in the human plasma pools, as detected by an indirect immunofluorescence assay (**Fig. 3a**). No noticeable recruitment of IgG was observed when RBCs were incubated with Nb-αDARC regardless of the plasma pools tested. A qualitative analysis performed by confocal microscopy confirmed that the fluorescence signal resulting from Nb-αDARC-P18F3-mediated IgG recruitment was located at the cell surface of RBCs (**Fig. 3b, c**).

Nb-αDARC-P18F3-mediated RBC opsonization triggers erythrophagocytosis by macrophage-like THP1 cells.

Engagement of FcγRI (CD64), FcγRIIa (CD32a) and FcγRIIIa (CD16a) present on monocytes and macrophages promotes phagocytosis of IgG-opsonized target cells[30]. Thus, to assess if anti-P18F3 huIgG recruited by Nb-αDARC-P18F3 bound to $DARC^+$ RBCs were able to promote RBC clearance by phagocytes, we performed an erythrophagocytosis assay using macrophage-like cells derived from the monocytic leukemia THP1 cell line ($CD64^+/CD32a^+/CD16a^-$) (**Supplementary Fig. 6**)[31].

Carboxyfluorescein succimidyl ester (CFSE)-stained $DARC^+$ RBCs were incubated for 3h at 37°C with macrophage-like cells (obtained by PMA treatment of THP1 cells) in presence of Nb-αDARC-P18F3 and of human plasma pools exhibiting low, intermediate, or high antibody titers against P18F3. Flow cytometry analysis of macrophage-like THP1 cells revealed that the percentage of $CFSE^+$ THP1 was largely increased when the cells were incubated with Nb-αDARC-P18F3 and a human plasma pool exhibiting a high titer of anti-P18F3 antibodies (**Fig. 4a**). When Nb-αDARC was used instead of Nb-αDARC-P18F3, no significant increase was observed (**Fig. 4a**). Four independent experiments confirmed that exposure of RBCs to Nb-αDARC-P18F3 and human plasma pools containing high or intermediate antibody titers against P18, provokes an increased erythrophagocytosis by THP1-derived macrophage-like cells (mean fold change 6.3 and 2.6, respectively) as compared to the condition using untreated RBCs (**Fig. 4b**). No increase was observed in absence of plasma in the assay where Nb-αDARC-P18F3 was used (**Fig. 4b**). Of note, erythrophagocytosis was more pronounced in presence of the plasma pool exhibiting the highest antibody titer against P18F3 (as compared to the "no plasma" condition; p=0.0286). In contrast, RBC treatment with Nb-αDARC did not modify the level of erythrophagocytosis directly exerted by macrophage-like THP1 cells, regardless of the plasma pools tested (**Fig. 4b**).

Altogether, these results identified P18F3 as the most efficient P18-derived polypeptide able to recruit specific IgG onto the cell surface of target cells. Fusion of P18F3 to a nanobody-based binding moiety (Nb-αDARC) did not alter the intrinsic functionality of the 2 modules and demonstrated a good capability to engage FcγRs on THP1-derived macrophages making it possible to recruit anti-P18 antibodies, present in human plasma, that trigger RBC phagocytosis.

Engineering a BMFP against human CD20.

We also developed a BMFP containing a scFv directed against huCD20 fused to the N-terminal end of P18F3 to target Burkitt's lymphoma cells *in vitro* and huCD20-expressing tumor cells in an *in vivo* mouse tumor model.

An anti-huCD20 scFv comprising the V_H domain fused to the V_κ domain with a $(GGGGS)_3$ interdomain linker, derived from the mouse IgG2b,κ 2H7 monoclonal antibody[32], was engineered (**Fig. 5a)** and expressed alone ($scFv_{2H7}$) or in fusion with P18F3 ($scFv_{2H7}$-P18F3) (**Fig. 5b and Supplementary Fig. 7**). Both constructs included a 6xHistidine tag (6xHis tag) at the C-terminus. The binding of the $scFv_{2H7}$ and $scFv_{2H7}$-P18F3 to native huCD20 expressed at the surface of cells from the Burkitt's lymphoma cell line RAJI (**Supplementary Fig. 8a**) was assessed by an indirect anti-His-tag fluorescence assay and flow cytometry (**Supplementary Fig. 8b**). Both $scFv_{2H7}$ and $scFv_{2H7}$-P18F3 bound to huCD20-expressing RAJI cells and a similar binding was observed when used at an equimolar concentration of 0.48 µM. As already observed with Nb-αDARC and Nb-αDARC-P18F3 (**Supplementary Fig. 4**), a difference in the binding curves of the two molecules was seen (**Supplementary Fig. 8b**). This may reflect a steric hindrance for the binding of the anti-6xHis antibody to the recombinant molecules when P18F3 is fused at their C-terminus rather than a change in the ability of BMFPs to bind the target molecules (DARC and huCD20).

ScFv$_{2H7}$-P18F3-mediated anti-P18 IgG opsonization of Burkitt's Lymphoma cells activates antibody-dependent complement cascade and triggers FcγRIIIa-mediated activation of intracellular signaling pathways.

We then evaluated if the binding of scFv$_{2H7}$-P18F3 to Burkitt's lymphoma cells induced the activation of the complement cascade in presence of a pool of heat-inactivated human plasma exhibiting a high titer of anti-P18F3 antibodies. This activation leads to the formation of the C5b-8 complex that binds to C9 to form the membrane attack complex (MAC), C5b-9. Incubation of RAJI cells with scFv$_{2H7}$-P18F3 in the presence of plasma led to more C5b-8/9 deposition than when untreated cells or cells coated with scFv$_{2H7}$ were tested as shown by an increased detection of C5b-8/9 using either rabbit anti-C5b-9 antibodies (Mann-Whitney test, p=0.0286) (**Fig. 5c**) or a mouse anti-C5b-8/9 mAb (**Supplementary Fig. 9a**).

The Fcγ region of immuno-complexed IgG can bind to FcγRIIIa/CD16a expressed at the surface of Natural Killer (NK) cells and trigger an intracellular signaling cascade leading to the release of IFN-γ, TNF-α and of perforin and granzymes from cytotoxic granules. Thus, we examined if scFv$_{2H7}$-P18F3-mediated anti-P18 IgG opsonization of Burkitt's Lymphoma cells could provoke the crosslinking of FcγRIIIa, hence triggering a signalling cascade that ultimately leads to ADCC. Jurkat cells stably expressing human FcγRIIIa-V158, that binds IgG1 more efficiently than FcγRIIIa-F158, were used as effector cells to monitor cell activation. In this reporter assay, FcγRIIIa engagement by immune-complexes transduces intracellular signals resulting in NFAT-mediated luciferase activity, which represents a robust and valid downstream readout for ADCC induction by IgG1 antibodies[33]. Thus, huCD20$^+$ RAJI cells were first opsonized with scFv$_{2H7}$-P18F3 or scFv$_{2H7}$ and then co-cultured with FcγRIIIa$^+$ Jurkat cells in presence of a pool of plasma

exhibiting a high titer of anti-P18F3 antibodies for 6 h. Treatment of RAJI cells with $scFv_{2H7}$-P18F3 drastically increased NFAT-mediated luciferase activity in Jurkat cells in the presence of plasma as compared to untreated cells or $scFv_{2H7}$-coated cells (**Fig. 5d and Supplementary Fig. 9b**), demonstrating that P18F3-mediated anti-P18 IgG opsonization of Burkitt' Lymphoma cells triggers FcγRIIIa-mediated activation of intracellular signaling pathways that leads to ADCC.

Treatment with $scFv_{2H7}$-P18F3 reduces cancer progression in mice bearing $huCD20^{+}$ tumor cells.

Firstly, in order to raise mouse antibodies directed against P18F3, 12 BALB/cByJ were immunized with the P18FL protein fused to MBP (MBP-P18FL). Analysis of IgG subclasses 52 days after the first injection revealed that around 46.8% of anti-P18F3 IgG are IgG1 and 34.9% IgG2b (mean values) (**Supplementary Fig. 10**). A smaller proportion of anti-P18 IgG belonged to the IgG3 and IgG2a subclasses (10.4% and 7.9%, respectively) (mean values). Individual pre-immune and immune sera from the 12 mice were then used to perform an opsonization assay with EL4-WT cells and transduced EL4-huCD20 cells that stably express human CD20[34] (**Supplementary Fig. 11a**). In the presence of immune mouse sera, binding of $scFv_{2H7}$-P18F3 to EL4-huCD20 cells led to the recruitment of anti-P18 mouse IgG as detected by an immunofluorescence assay using specific goat anti-mouse IgG (Fc-specific) antibodies conjugated to allophycocyanine (APC) and hence, to opsonization of target cells (**Fig. 6a, right panel**). No noticeable recruitment of IgG was observed without scFv (**Fig. 6a, left panel**), when the $scFv_{2H7}$ was tested (**Fig. 6a, middle panel**) and when EL4-WT were treated with $scFv_{2H7}$ or $scFv_{2H7}$-P18F3 and incubated with pre-immune sera (**Supplementary Fig. 11b, middle and right panels**).

Second, to determine whether or not $scFv_{2H7}$-P18F3 therapy can protect mice from tumor challenge, C57Bl/6 immunocompetent mice were immunized with MBP-P18FL to generate endogenous anti-P18 antibodies (**Fig. 6b**). Mice were then injected intravenously with 2.5 x 10^5 EL4-huCD20 cells (Day 0) and received $scFv_{2H7}$-P18F3 therapy (group G1.1), consisting in four intraperitoneal injections at days 1, 4, 7 and 10. In a first set of experiments, 3 additional control groups (n=5) were injected with tumor cells. Mice from group G1.2 were left untreated, whereas mice from group G1.3 received 4 injections of $scFv_{2H7}$. Mice from group G1.4 received $scFv_{2H7}$-P18F3 therapy but were not pre-immunized with MBP-P18FL (**Fig. 6c**). All mice from G1.2, G1.3 and G1.4 died within 35-50 days post tumor cell injection. In contrast, the overall long-term survival in the G1.1 group ($scFv_{2H7}$-P18F3 therapy) was 40% (**Fig. 6c**). In a second set of experiments involving a larger number of animals, 2 groups were designed. The G2.1 group (n=11) did not receive any treatment after injection of tumor cells whereas the animals from the G2.2 group (n=12) received $scFv_{2H7}$-P18F3 therapy (**Fig. 6d**). All mice from the untreated group died before Day 60 (median survival 35 days). $ScFv_{2H7}$-P18F3 therapy significantly increased mice survival (median survival 51.5 days; Log-rank Mantel-Cox test, p=0.0387) and led to an overall 17% long-term survival. Two days before EL4-huCD20 cell injection, most of circulating anti-P18F3 IgG in mice from G1.1 and G2.1 belonged to the IgG1 and IgG2b subclasses (**Fig. 6c, 6d – right panels**) as already observed in sera from MBP-P18FL-immunized mice used to test IgG opsonization (**Supplementary Fig. 10**). In addition, $scFv_{2H7}$-P18F3 treatment led to increased levels of circulating antibodies directed against P18F3 at Day 15 post-treatment (**Supplementary Fig. 12**).

DISCUSSION

Here, we describe a strategy for re-directing a pre-existing EBV antibody response towards defined pathogenic cells using bi-modular fusion proteins comprising a specific binding moiety and an EBV-derived Ig recruiting antigen, P18. As a proof of concept, we first generated a set of BMFPs targeting RBCs via an anti-DARC nanobody. Treatment of RBCs with BMFPs in presence of human plasma from EBV^+ donors mediated target opsonization by circulating anti-P18 IgG and the subsequent induction of erythrophagocytosis by macrophage-like cells. We then developed a scFv-based BMFP directed towards huCD20 ($scFv_{2H7}$-P18F3) and analysed its efficacy *in vitro* and *in vivo* in a mouse tumour model. $ScFv_{2H7}$-P18F3-mediated opsonization of Burkitt's lymphoma cells, activated the antibody-dependent cascade of the complement system and engaged FcγRIII in a cell assay recapitulating the first steps of ADCC triggering. When assessed in a tumour model, $scFv_{2H7}$-P18F3 therapy significantly increased mice survival, leading to total cancer remission in some animals.

The initial part of this work consisted in establishing that BMFPs, expressed in a bacteria-based system, could be designed to efficiently target defined cellular elements. The conservation of the intrinsic biochemical and functional properties of both modules (P18 and binding moiety), is crucial when designing BMFPs aiming at re-directing a pre-existing EBV antibody response towards specific cells. In order to create a versatile therapeutic tool, in which the binding moiety could be easily substituted, we first optimized the nature of the P18 antigen using a model targeting DARC expressed at the surface of RBCs with a nanobody-based BMFP (Nb-αDARC). The EBV antigen P18 has been selected primarily for its capability to be strongly bound by circulating IgG from EBV-infected individuals[18]. Another important criterion for selecting P18 was the absence of any post-translational addition of sugar moieties. P18 is a non-glycosylated protein of small size (18 kDa) that could therefore be produced in a heterologous bacterial system. However, protein

sequence analysis of P18FL revealed that its N-terminus part displays several stretches of hydrophobic residues and numerous prolines that could potentially interfere with the expression of stable proteins in physiological buffers. Furthermore, P18FL harbors a cysteine in position 56 that could unwillingly engage in disulfide bond formation with other cysteines present within the binding moiety sequence during folding of the fusion constructs as antibody fragments possess structuring disulfide-bonds mandatory for their functionality. To overcome these potential issues, we designed P18 fragments lacking the N-terminus region that contains Cys56. In addition, we used a mutant *E. coli* strain (SHuffle) that promotes disulfide bond formation in the cytoplasm, leading to more efficient folding of recombinant proteins, improved activity and increased production yields[29]. We also optimized the P18 antigen to efficiently recruit circulating anti-P18 IgG, without affecting the functionality of the binding moiety. P18F3 was down-selected as the prime P18-derived antigen, presenting binding titers by circulating anti-P18 IgG comparable to that of P18FL, thus confirming the presence of immunodominant epitopes within the C-terminus part of the protein[35]. Notably, fusion of P18F3 to Nb-αDARC did not significantly affect the affinity of the Nb for its cognate target, DARC. Furthermore, RBC treatment with Nb-αDARC-P18F3 triggered erythrophagocytosis by THP1-derived macrophages. The amplitude of erythrophagocytosis correlated with the P18F3-binding titers of the circulating IgG, strongly suggesting that erythrophagocytosis was driven by IgG opsonization rather than by pattern recognition receptors or mannose receptor engagement.

Based on these results, we then generated a P18F3-derived BMFP comprising a scFv binding moiety targeting huCD20 that is expressed at the surface of B lymphocytes from early developmental stages (late pro-B cell) to late stages (memory B cell) as well as in most non-Hodgkin's B lymphomas. MAb therapy targeting huCD20 has revolutionized the treatment of B-

cell malignancies for more than 30 years, becoming the leading therapeutic agents for the care of numerous B cell-related cancers such as follicular lymphoma, diffuse large B-cell lymphoma, mantle cell lymphoma as well as Burkitt's lymphoma[36]. The most striking example of such success is rituximab[37]. Several other therapeutic anti-huCD20 mAbs such as ofatumumab, obinutuzumab, and ublituximab (derived from the EMAB-6 antibody[38]) have been developed since the advent of rituximab (with alternate binding epitopes, additional humanization and modified glycosylations)[39,40]. We have developed herein a binding moiety targeting the large extracellular loop of huCD20 based on the C2H7 (2H7) chimeric antibody, which presents a different binding epitope profile than rituximab[41]. $ScFv_{2H7}$-P18F3 expression in SHuffle resulted in the production of a soluble protein, with a production yield reaching 0.7-1 mg ml^{-1} of bacteria culture, in line with previous work highlighting the difficulty to express stable and soluble scFv molecules[42,43]. We demonstrate here that treatment of Burkitt's lymphoma cells with $scFv_{2H7}$-P18F3, in the presence of plasma from EBV^+ donors, activates the complement cascade leading to the formation of the MAC as shown by the detection of C5b-9 deposition at the cell surface. The ability of the $scFv_{2H7}$-P18F3 to trigger the MAC formation and deposit on target cells strongly supports the relevance of BMFP-based treatments to deplete pathologic cells. Several *in vivo* studies have highlighted that complement activation is important for the therapeutic activity of depleting antibodies, as exemplified by anti-huCD20 mAbs[34,44]. Importantly, in addition to complement activation, $scFv_{2H7}$-P18F3-mediated opsonization also provoked the engagement of FcγRIII at the surface of engineered Jurkat cells in presence of plasma from EBV^+ individuals, triggering the first steps of the signaling cascade leading to ADCC. Thus, these data indicate that anti-huCD20 BMFPs used in EBV^+ patients could enable the recruitment of endogenous anti-P18 IgG at the surface of $huCD20^+$ B cells, leading to the triggering of immune effector mechanisms. The continuous

bioavailability of endogenous polyclonal IgG could represent a strong benefit to improve engagement of the C1q complement component and of FcγRs, thus leading to a sustained therapeutic efficacy. The *in vivo* anti-tumor efficacy of scFv$_{2H7}$-P18F3 therapy was therefore assessed in a mouse model. Early attempts in the late seventies to develop *in vivo* EBV models by virus inoculation of non-human primates did not result in asymptomatic persistent infections[45]. Since then, humanized mice, which can recapitulate key aspects of EBV infection observed in humans have been established[46,47]. However, these models are arduous to implement and still face some severe limitations including sub-optimal IgG responses[48]. To assess the anti-tumor activity of scFv$_{2H7}$-P18F3 *in vivo* in presence of anti-P18 antibodies, we used a mouse tumor model, in which cells expressing human CD20 (EL4-huCD20) served as tumor target cells[25,26,44,49]. Mice were first pre-immunized with MBP-P18FL to generate circulating anti-P18F3 antibodies. Following EL4-huCD20 injection, preimmunized mice who received a scFv$_{2H7}$-P18F3 therapy showed a protection against tumor development as shown by an increased survival time and by the full tumor clearance observed in 17% to 40% of the animals. Analysis of the mouse IgG subclasses specific to P18F3 induced by MBP-P18FL immunization, revealed a predominance of IgG1, and to a lower extent, of IgG2b. In contrast to human IgG1s, mouse IgG1s are poorly able to bind C1q or to engage activating FcγRs. Conversely, this subclass can efficiently bind to the inhibitory FcγRIIb. Thus, it is important to stress that despite these marked limitations, the efficacy of scFv$_{2H7}$-P18F3 therapy, obtained after 4 injections of only 57 µg of BMFP (per injection), is achieved in less favorable conditions than in humans, where human IgG1, the major component of the anti-P18 antibody response, exhibits strong effector functions through the binding to C1q and activating FcγRs. Of note, the protection observed was obtained with a cumulative dose of 228 µg of the recombinant fusion BMFP, whereas previous work[31,32,33], that used the same mouse

388 tumor model, required a cumulative dose of 1 mg of an IgG2a anti-huCD20 mouse mAb, the most
389 effective mouse subclass to engage FcγRs and to activate complement. Interestingly $scFv_{2H7}$-
390 P18F3 treatment allowed the recall of the P18F3 antibody response, which could serve as a booster
391 in patients presenting low anti-P18F3 IgG titers.
392
393 Overall, EBV-derived bi-modular fusion proteins represent a versatile therapeutic tool for re-
394 directing an Epstein-Barr virus pre-existing antibody response towards defined target cells. Their
395 main advantages over the use of therapeutic depleting/cytotoxic mAbs are (i) the flexibility of the
396 constructs in terms of binding moieties that can be easily made of antibody fragments with various
397 specificities such as scFv, nanobodies or other types of ligands directed against a specific cell
398 surface receptor, ii) the lack of Fc region, rendering unnecessary any further Fc engineering for
399 gaining optimized effector functions due to the recruitment of polyclonal anti-P18 IgG1 exhibiting
400 excellent cytotoxic properties (CDC and ADCC), (iii) the reduced doses to be injected due to the
401 recruitment of polyclonal endogenous IgG, mostly IgG1, directed against P18, a mechanism that
402 will amplify the efficacy of antibody-mediated effector functions, iv) a continuous bioavailability
403 of endogenous polyclonal effector IgG, v) the ability to produce large amounts of bi-modular
404 fusion proteins using bacteria and not eukaryotic cells, with reduced costs of production.

REFERENCES

1. Lu, R.-M. *et al.* Development of therapeutic antibodies for the treatment of diseases. *J. Biomed. Sci.* **27**, 1 (2020).
2. Chiu, M. L., Goulet, D. R., Teplyakov, A. & Gilliland, G. L. Antibody Structure and Function: The Basis for Engineering Therapeutics. *Antibodies.* **8**, (2019).
3. Kang, T. H. & Jung, S. T. Boosting therapeutic potency of antibodies by taming Fc domain functions. *Exp. Mol. Med.* **51**, 1–9 (2019).
4. Wang, X., Mathieu, M. & Brezski, R. J. IgG Fc engineering to modulate antibody effector functions. *Protein Cell* **9**, 63–73 (2018).
5. Gramer, M. J. *et al.* Modulation of antibody galactosylation through feeding of uridine, manganese chloride, and galactose. *Biotechnol. Bioeng.* **108**, 1591–1602 (2011).
6. Diebolder, C. A. *et al.* Complement is activated by IgG hexamers assembled at the cell surface. *Science* **343**, 1260–1263 (2014).
7. Shields, R. L. *et al.* Lack of fucose on human IgG1 N-linked oligosaccharide improves binding to human Fcgamma RIII and antibody-dependent cellular toxicity. *J. Biol. Chem.* **277**, 26733–26740 (2002).
8. Mimoto, F. *et al.* Novel asymmetrically engineered antibody Fc variant with superior FcγR binding affinity and specificity compared with afucosylated Fc variant. *mAbs* **5**, 229–236 (2013).
9. Sibéril, S. *et al.* Selection of a human anti-RhD monoclonal antibody for therapeutic use: impact of IgG glycosylation on activating and inhibitory Fc gamma R functions. *Clin. Immunol.* **118**, 170–179 (2006).

10. Beliard, R. *et al.* A human anti-D monoclonal antibody selected for enhanced FcgammaRIII engagement clears RhD+ autologous red cells in human volunteers as efficiently as polyclonal anti-D antibodies. *Br. J. Haematol.* **141**, 109–119 (2008).
11. Richards, J. O. *et al.* Optimization of antibody binding to FcgammaRIIa enhances macrophage phagocytosis of tumor cells. *Mol. Cancer Ther.* **7**, 2517–2527 (2008).
12. Dall'Acqua, W. F., Kiener, P. A. & Wu, H. Properties of human IgG1s engineered for enhanced binding to the neonatal Fc receptor (FcRn). *J. Biol. Chem.* **281**, 23514–23524 (2006).
13. Robbie, G. J. *et al.* A novel investigational Fc-modified humanized monoclonal antibody, motavizumab-YTE, has an extended half-life in healthy adults. *Antimicrob. Agents Chemother.* **57**, 6147–6153 (2013).
14. Hendrikx, J. J. M. A. *et al.* Fixed Dosing of Monoclonal Antibodies in Oncology. *The Oncologist* **22**, 1212–1221 (2017).
15. Young, L. S. & Rickinson, A. B. Epstein–Barr virus: 40 years on. *Nat. Rev. Cancer* **4**, 757–768 (2004).
16. Babcock, G. J., Decker, L. L., Volk, M. & Thorley-Lawson, D. A. EBV persistence in memory B cells in vivo. *Immunity* **9**, 395–404 (1998).
17. Thorley-Lawson, D. A. EBV Persistence—Introducing the Virus. in *Epstein Barr Virus Volume 1* (ed. Münz, C.) vol. 390 151–209 (Springer International Publishing, 2015).
18. Ogolla, S. *et al.* Reduced Transplacental Transfer of a Subset of Epstein-Barr Virus-Specific Antibodies to Neonates of Mothers Infected with Plasmodium falciparum Malaria during Pregnancy. *Clin. Vaccine Immunol.* **22**, 1197–1205 (2015).
19. Kaplon, H. & Reichert, J. M. Antibodies to watch in 2021. *mAbs* **13**, 1860476 (2021).

20. Merle, N. S., Church, S. E., Fremeaux-Bacchi, V. & Roumenina, L. T. Complement System Part I - Molecular Mechanisms of Activation and Regulation. *Front. Immunol.* **6**, 262 (2015).
21. Merle, N. S., Noe, R., Halbwachs-Mecarelli, L., Fremeaux-Bacchi, V. & Roumenina, L. T. Complement System Part II: Role in Immunity. *Front. Immunol.* **6**, 257 (2015).
22. Nimmerjahn, F. & Ravetch, J. V. Fcγ receptors as regulators of immune responses. *Nat. Rev. Immunol.* **8**, 34–47 (2008).
23. Hogarth, P. M. & Pietersz, G. A. Fc receptor-targeted therapies for the treatment of inflammation, cancer and beyond. *Nat. Rev. Drug Discov.* **11**, 311–331 (2012).
24. Anthony, R. M. *et al.* Recapitulation of IVIG anti-inflammatory activity with a recombinant IgG Fc. *Science* **320**, 373–376 (2008).
25. Abès, R., Gélizé, E., Fridman, W. H. & Teillaud, J.-L. Long-lasting antitumor protection by anti-CD20 antibody through cellular immune response. *Blood* **116**, 926–934 (2010).
26. DiLillo, D. J. & Ravetch, J. V. Differential Fc-Receptor Engagement Drives an Anti-tumor Vaccinal Effect. *Cell* **161**, 1035–1045 (2015).
27. Horuk, R. The Duffy Antigen Receptor for Chemokines DARC/ACKR1. *Front. Immunol.* **6**, 279 (2015).
28. Smolarek, D. *et al.* A recombinant dromedary antibody fragment (VHH or nanobody) directed against human Duffy antigen receptor for chemokines. *Cell. Mol. Life Sci. CMLS* **67**, 3371–3387 (2010).
29. Lobstein, J. *et al.* SHuffle, a novel Escherichia coli protein expression strain capable of correctly folding disulfide bonded proteins in its cytoplasm. *Microb. Cell Factories* **11**, 56 (2012).

30. Uribe-Querol, E. & Rosales, C. Phagocytosis: Our Current Understanding of a Universal Biological Process. *Front. Immunol.* **11**, 1066 (2020).
31. Tsuchiya, S. *et al.* Establishment and characterization of a human acute monocytic leukemia cell line (THP-1). *Int. J. Cancer* **26**, 171–176 (1980).
32. Liu, A. Y. *et al.* Production of a mouse-human chimeric monoclonal antibody to CD20 with potent Fc-dependent biologic activity. *J. Immunol. 1950* **139**, 3521–3526 (1987).
33. Parekh, B. S. *et al.* Development and validation of an antibody-dependent cell-mediated cytotoxicity-reporter gene assay. *mAbs* **4**, 310–318 (2012).
34. Di Gaetano, N. *et al.* Complement activation determines the therapeutic activity of rituximab in vivo. *J. Immunol. 1950* **171**, 1581–1587 (2003).
35. van Grunsven, W. M., Spaan, W. J. & Middeldorp, J. M. Localization and diagnostic application of immunodominant domains of the BFRF3-encoded Epstein-Barr virus capsid protein. *J. Infect. Dis.* **170**, 13–19 (1994).
36. Casan, J. M. L., Wong, J., Northcott, M. J. & Opat, S. Anti-CD20 monoclonal antibodies: reviewing a revolution. *Hum. Vaccines Immunother.* **14**, 2820–2841 (2018).
37. Salles, G. *et al.* Rituximab in B-Cell Hematologic Malignancies: A Review of 20 Years of Clinical Experience. *Adv. Ther.* **34**, 2232–2273 (2017).
38. de Romeuf, C. *et al.* Chronic lymphocytic leukaemia cells are efficiently killed by an anti-CD20 monoclonal antibody selected for improved engagement of FcgammaRIIIA/CD16. *Br. J. Haematol.* **140**, 635–643 (2008).
39. Soe, Z. N. & Allsup, D. The use of ofatumumab in the treatment of B-cell malignancies. *Future Oncol.* **13**, 2611–2628 (2017).

40. Prica, A. & Crump, M. Improving CD20 antibody therapy: obinutuzumab in lymphoproliferative disorders. *Leuk. Lymphoma* **60**, 573–582 (2019).
41. Du, J. *et al.* Crystal structure of chimeric antibody C2H7 Fab in complex with a CD20 peptide. *Mol. Immunol.* **45**, 2861–2868 (2008).
42. Wang, R. *et al.* Engineering production of functional scFv antibody in E. coli by co-expressing the molecule chaperone Skp. *Front. Cell. Infect. Microbiol.* **3**, 72 (2013).
43. Sarker, A., Rathore, A. S. & Gupta, R. D. Evaluation of scFv protein recovery from E. coli by in vitro refolding and mild solubilization process. *Microb. Cell Factories* **18**, 5 (2019).
44. Golay, J. *et al.* The role of complement in the therapeutic activity of rituximab in a murine B lymphoma model homing in lymph nodes. *Haematologica* **91**, 176–183 (2006).
45. Miller, G. *et al.* Lymphoma in cotton-top marmosets after inoculation with Epstein-Barr virus: tumor incidence, histologic spectrum antibody responses, demonstration of viral DNA, and characterization of viruses. *J. Exp. Med.* **145**, 948–967 (1977).
46. Yajima, M. *et al.* A new humanized mouse model of Epstein-Barr virus infection that reproduces persistent infection, lymphoproliferative disorder, and cell-mediated and humoral immune responses. *J. Infect. Dis.* **198**, 673–682 (2008).
47. Fujiwara, S., Imadome, K.-I. & Takei, M. Modeling EBV infection and pathogenesis in new-generation humanized mice. *Exp. Mol. Med.* **47**, e135 (2015).
48. Akkina, R. New generation humanized mice for virus research: comparative aspects and future prospects. *Virology* **435**, 14–28 (2013).
49. Deligne, C., Metidji, A., Fridman, W.-H. & Teillaud, J.-L. Anti-CD20 therapy induces a memory Th1 response through the IFN-γ/IL-12 axis and prevents protumor regulatory T-cell expansion in mice. *Leukemia* **29**, 947–957 (2015).

ACKNOWLEDGMENTS

This work was supported by a grant from the SATT IDF-Innov, Paris, France. Additional financial support was provided by the Institut National de la Santé et de la Recherche Médicale (INSERM), France and the Institut National de la Transfusion Sanguine (INTS), Paris, France. We are thankful to Dr. Dominique Goossens, Dr. Zelia Gouveia, Ms Nathalie Josseaume for providing reagents, to Mr Mickael Marin, Ms Sandy Peltier for technical assistance and to Dr. Geneviève Milon for inspiring discussions.

AUTHOR CONTRIBUTIONS

BG, OB, SG, JLT, AC designed the research study. CB, NR, BKD, CEP, AD, JC, JPS, AC performed the experiments and analyzed the data. BG, JLT, AC wrote the first version of the manuscript. All authors critically reviewed and validated the submitted version of the manuscript.

COMPETING INTERESTS

BG, SG and AC declare being listed as co-inventors of an international patent application published under the patent cooperation treaty (PCT), WO2017/103020A1. The other authors declare no competing interests.

SUPPLEMENTARY INFORMATION

Supplementary information accompanies this paper.

ONLINE METHODS

Production and purification of MBP-P18FL, DARC-ECD1 and DARC-Mut

Genomic EBV DNA (strain B95-8) was isolated from cells of the marmoset (*Callithrix jacchus*) cell line B95-8 (ECACC). The complete DNA sequences of the ORF BFRF3 encoding for the viral capsid antigens P18 (UniProt P03197; aa 1-176) was cloned into the pMal-C2x plasmid (New England Biolabs) suitable for expression of maltose-binding protein (MBP)-fusions. The sequences coding for the extracellular domain of DARC (DARC-ECD1) and the CA52 epitope-mutated form of this domain (DARC-ECD1-Mut), which is no longer recognized by the anti-DARC nanobody (**Supplementary Fig. 3),** were cloned into the pGEX-5 plasmid (GE Healthcare). For protein expression, BL21 competent *E. coli* (New England Biolabs) were transformed with pMal-C2x-P18, the empty pMal-C2x plasmid (MBP alone), pGEX-5- DARC-ECD1 as well as with pGEX-5-DARC-ECD1-Mut. Bacteria cultures were grown at 37°C until OD_{600nm} 0.5 and protein expression was carried out for 3 h at 37°C with 0.1 mM isopropyl β-d-1-thiogalactopyranoside (IPTG) (Sigma). The bacteria pellets were resuspended in 50 mM Tris, 500 mM NaCl at pH 7.2 and frozen at -80°C until further use. For protein purification, bacteria suspensions were thawed on ice and supplemented with ethylenediaminetetraacetic acid (EDTA)-free *cOmplete Protease Inhibitors* (Roche) and with 1 mg ml^{-1} lysozyme from chicken egg white (Sigma). Bacteria lysis was achieved by passing the cell suspensions through an EmulsiFlex-C5 high-pressure homogenizer (Avestin), three times at 4°C. Following centrifugation at 12,000 x *g*, the supernatants containing soluble proteins were subjected to a 2-step purification process. MBP-fusion proteins were first purified on Amylose resin (New England Biolabs) whereas GST-fusion proteins were purified on glutathione sepharose 4 Fast Flow (GE healthcare) according to manufacturer's instructions. Purified proteins were then passed through a Superdex 200 10/300

GL gel filtration column (GE Healthcare) in phosphate-buffered saline (PBS) (Gibco) at pH 7.2. Double-purified proteins were snap-frozen in liquid nitrogen and stored at -80°C.

BMFPs cloning, expression and purification

The DNA sequence ORF BFRF3 encoding for P18 was recoded and optimized for *E. coli* codon usage (Integrated DNA Technology) to allow maximal expression in *E. coli*-based systems. The full-length P18 (P18FL) recoded sequence as well as the truncated fragment (P18F2, P18F3, P18F4) sequences were cloned into a pet28a-derived plasmid (Novagen) in order to express C-terminus His-tagged proteins.

The anti-human CD20 (huCD20) V_H and V_κ sequences of $scFv_{2H7}$ were obtained from the sequences of an anti-human-CD28 x anti-huCD20 bispecific scFv antibody (clone r2820) (Genebank AJ937362) and synthesized according to the following orientation: V_H-$(GGGGS)_3$-V_κ. The DNA sequences of Nb-αDARC and $scFv_{2H7}$ were inserted between the NheI and NcoI restriction sites of Pet28a-NC (**Supplementary Fig. 2**). For each BMFP set, a construct comprising the binding moiety but lacking P18 was also generated.

For protein expression, *E. coli* SHuffle (New England Biolabs) were transformed with the different constructs. Bacteria cultures were induced with 0.2 mM IPTG at OD_{600nm} 0.8 and protein expression was carried out at 20°C for 16 h. The bacteria pellets were resuspended in 50 mM Tris, 500 mM NaCl at pH 7.2 and the samples were then frozen at -80°C until further use. For protein purification, bacteria suspensions were thawed on ice and supplemented with EDTA-free *cOmplete Protease Inhibitors* (Roche) and with 1 mg ml^{-1} lysozyme from chicken egg white (Sigma). Bacteria lysis was achieved by passing the cell suspensions through an EmulsiFlex-C5 high-pressure homogenizer (Avestin), three times at 4°C. Following centrifugation at 12,000 x *g*,

583 the supernatants containing soluble proteins were subjected to a 2-step purification process. His-
584 tagged proteins were first purified on Ni-NTA Superflow columns (Qiagen) according to
585 manufacturer's instructions and then passed through a Superdex 200 10/300 GL gel filtration
586 column (GE Healthcare) in PBS at pH 7.2. Purified proteins were snap-frozen in liquid nitrogen
587 and stored at -80°C.
588
589 **Blood samples.** Whole blood samples were collected at the Etablissement Français du Sang (EFS)-
590 Cabanel, Paris, France (convention number CCPSLUNT-N°12/EFS/135). Red blood cells (RBCs)
591 and plasma samples were recovered after centrifugation of whole blood at 300 x *g* for 10 min.
592 When required, complement inactivation was achieved by heating plasma samples at 56°C for 30
593 min. $DARC^+$ RBCs from individuals with the FY^{a+}/FY^{b+} genotype were obtained from a reference
594 panel provided by the Centre National de Référence pour les Groupes Sanguins (CNRGS), Paris,
595 France.
596
597 **Cell lines.** The marmoset B95-8 cells that produce infectious EBV particles, the human
598 lymphoblastoid RAJI B cells (ECACC) and the human monocytic leukemia THP1 cells (ECACC)
599 were cultured in RPMI 1640 (Gibco), 2mM glutamine (Gibco), 10% heat-inactivated Fetal Bovine
600 Serum (FBS) (Dominique Dutcher), penicillin-streptomycin (100 U/ml) at 37°C, 5% CO_2. EL4-
601 WT (ECACC) and EL4-huCD20 (kindly provided by Dr. J. Golay, Bergamo, Italy) cells were
602 maintained in DMEM (Gibco) supplemented with 2mM glutamine (Gibco), 20% FBS, penicillin-
603 streptomycin (100 U/ml) at 37°C, 5% CO_2.
604

Surface plasmon resonance studies of the binding of anti-DARC BMFPs to recombinant DARC-ECD1. Interactions between the anti-DARC BMFPs and DARC were studied by surface plasmon resonance (SPR), using a Biacore X100 instrument (GE Healthcare). All experiments were performed in HBS-EP buffer (GE Healthcare) at 25°C. For studying the binding of Nb-αDARC, Nb-αDARC-P18F2, Nb-αDARC-P18F3, Nb-αDARC-P18F4 to DARC, DARC-ECD1 was immobilized on the analysis Fc2 channel of a CM5 chip (GE Healthcare) by amine coupling whereas DARC-ECD1-Mut was immobilized on the reference channel Fc1. Both channels were then blocked with 1 M ethanolamine-HCl pH 8.5. BMFPs were injected at 30 µl min^{-1} in dilution series (0.1 to 125 µM) over the coated chips. Between the injections, the chip surface was regenerated with 2 injections of 15 µl of 10 mM HCl pH 2.0. The specific binding responses to the molecular targets were obtained by subtracting the response given by the analytes on Fc2 with the response on Fc1. The kinetic sensorgrams were fitted to a global 1:1 interaction Langmuir model and the K_{off} and K_{on} values were calculated using the manufacturer's software (Biacore X100 Evaluation version 2.0).

Immune recognition of BMFPs by anti-P18 IgG-containing human plasma. Ultra-high binding flat-bottom microtiter 96-well plates (Immulon 4HBX) were coated overnight at 4°C with 100 µl of anti-DARC or anti-huCD20 BMFPs at 1 µg ml^{-1} in PBS. Plates were then washed 3 times with 200 µl PBS and blocked for 1 h at RT with 100 µl of PBS 1% bovine serum albumin (BSA) (Sigma). After blocking solution removing, three-fold serial dilutions (1/2 to 1/354,294) of human plasma were added into the wells and incubated for 1 h at RT. Plates were then washed three times with PBS. One hundred microliters of AffiniPure $F(ab')_2$ fragment donkey anti-human IgG(Fcγ) Horseradish Peroxidase-conjugated antibody (Jackson Immunoresearch) diluted 1/4,000

in PBS 1% BSA were added to each well and incubated for 45 min at RT. Plates were then washed three times with PBS and 100 µl of TMB (3,3',5,5'-tetramethylbenzidine) substrate (Biorad) were added per well. Absorbance was measured at 655 nm on an iMARK microplate absorbance reader (Biorad). Data (OD_{655nm}) were plotted and subjected to 4-parameter logistic regression curve fitting.

Binding of BMFPs to native molecular targets. Target cells (2.5×10^5) (RBCs, RAJI cells, EL4-WT, or EL4-huCD20 cells depending on the BMFPs tested) were distributed in a 96-well, round-bottom, polystyrene microplate (Corning 3798) pre-coated with PBS 1% BSA for 1 h at RT. To prevent non-specific binding, cells were incubated with PBS 1% BSA for 1 h at 4°C. Cells were then pelleted by centrifugation at 300 x *g* for 3 min at 4°C and resuspended in 100 µl of PBS 1% BSA containing BMFPs at various concentrations. Following 1 h incubation at 4°C, cells were washed three times with 200 µl PBS 1% BSA and resuspended in 100 µl of PBS 1% BSA containing 0.5 µg of purified mouse anti-$(H)_5$ (Penta-His) (Qiagen). After 45 min, cells were washed three times with 200 µl PBS 1% BSA and resuspended in 100 µl of PBS 1% BSA containing AffiniPure $F(ab')_2$ fragment goat anti-mouse IgG (H+L) PE-conjugated (1/100) (Jackson Immunoresearch). After 45 min, cells were washed three times with 200 µl PBS and subjected to flow cytometry analysis in the presence of TO-PRO®-3 (Molecular probes) diluted 1/10,000. Data acquisition was performed using BD FACSCanto™ II flow cytometer (Becton-Dickinson). Target cell gating was performed based on morphological features using the forward (FSC) and side (SSC) scatters. TO-PRO®-3 positive dead cells were excluded. Data were then analyzed in FLOWJO 8.1 (Tree Star Inc.) software.

651 **Anti-DARC BMFPs-mediated opsonization of RBCs.** Target cells (2.5 x 10^5 RBCs) were
652 distributed in a 96-well plate pre-coated with PBS 1% BSA for 1 h at RT. To prevent non-specific
653 binding, RBCs were incubated with PBS 1% BSA for 1 h at 4°C. Cells were then pelleted and
654 resuspended in 100 µl of PBS 1% BSA containing 9.6 nM Nb-αDARC-P18F3. Following 1 h
655 incubation at 4°C, RBCs were washed three times with 200 µl PBS 1% BSA and resuspended in
656 100 µl of human plasma pools diluted from 1/5 to 1/10,240 in PBS 1%. After 1 h, cells were
657 washed three times with 200 µl PBS 1% BSA and resuspended in 100 µl of PBS 1% BSA
658 containing AffiniPure $F(ab')_2$ fragment donkey anti-human IgG (Fc) PE-conjugated (1/100)
659 (Jackson Immunoresearch). After 45 min, RBCs were washed three times with 200 µl PBS and
660 subjected to flow cytometry.
661
662 **Antibody-dependent phagocytosis (ADP).** THP1 cells were differentiated into M0 macrophage-
663 like cells with phorbol 12-myristate 13-acetate (PMA) (Sigma). Briefly, THP1 cells were seeded
664 in 12-well plates (7.5 x 10^5 cells/well) and incubated for 48 h at 37°C, 5% CO_2 in complete medium
665 supplemented with 20 ng/ml PMA. FY^+ human RBCs were stained with Carboxyfluorescein
666 succinimidyl ester (CFSE) (Thermo Fisher) according to manufacturer's instructions. Stained
667 RBCs were incubated for 1 h at RT with Nb-αDARC-18F3 or with Nb-αDARC at saturating
668 concentrations in PBS 1% BSA and subsequently with human plasma pools diluted 1/10 in PBS
669 1% BSA. Opsonized RBCs were then incubated for 3 h at 37°C, 5% CO_2 with THP1-derived
670 macrophages-like at an effector/target cell (E/T) ratio of 1/100. After co-incubation, non-
671 phagocytized RBCs were lysed with RBC lysis buffer (ChemCruz) and macrophages-like cells
672 were subjected to flow cytometry analysis in presence of TO-PRO®-3 diluted 1/10,000. $CFSE^+$
673 macrophages-like cells were considered as cells having phagocytized at least one RBC.

674

675 **Activation of complement cascade.** Target RAJI cells (2.5 x 10^5) were distributed in a 96-well
676 plate pre-coated with PBS 1% BSA for 1 h at RT. To prevent non-specific binding, cells were
677 incubated with PBS 1% BSA for 1 h at 4°C. Cells were then pelleted and resuspended in 100 µl of
678 PBS 1% BSA containing $scFv_{2H7}$-P18F3 or $scFv_{2H7}$ at 0.48 µM. Following 1 h incubation at 4°C,
679 cells were washed three times with 200 µl PBS 1% BSA and resuspended in 100 µl of undiluted
680 heat-inactivated (56°C, 30 min) or untreated plasma. After a 1 h incubation at 37°C, cells were
681 washed three times with 200 µl PBS 1% BSA and resuspended in 100 µl of PBS 1% BSA
682 containing purified mouse (IgG2a, κ) anti-C5b-9 + C5b-8 [aE11] (20 µg ml^{-1}) or rabbit polyclonal
683 anti-C5b-9 (25 µg ml^{-1}) (Abcam). After 45 min at 4°C, cells were washed three times with 200
684 µl PBS 1% BSA and resuspended in 100 µl of PBS 1% BSA containing APC-conjugated goat anti-
685 mouse IgG (Fcγ fragment specific) (1/100) or PE-conjugated donkey anti-rabbit IgG (H+L)
686 (1/100) (Jackson Immunoresearch). After 20 min at 4°C, cells were washed three times with 200
687 µl PBS and subjected to flow cytometry analysis.
688

689 **Triggering of early events of Antibody-Dependent Cell-mediated Cytotoxicity (ADCC).**
690 $ScFv_{2H7}$-P18F3-mediated triggering of early events of ADCC was monitored using the reporter
691 Bioassay Core Kit (Promega) according to manufacturer's instructions. Target RAJI cells (12,500)
692 were distributed in a 96-well plate pre-coated with PBS 1% BSA for 1 h at RT. To prevent non-
693 specific binding, cells were incubated with PBS 1% BSA for 1 h at 4°C. Cells were then pelleted
694 and resuspended in 100 µl of PBS 1% BSA containing $scFv_{2H7}$-P18F3 or $scFv_{2H7}$ at 0.48 µM.
695 Following 1 h incubation at 4°C, cells were washed three times with 200 µl PBS 1% BSA and
696 resuspended in ADCC Assay Buffer containing heat-inactivated (56°C, 30 min) human plasma at

different dilutions. Effector FcγRIII^{+} Jurkat cells (75,000) were added into each well. Plates were incubated at 37°C, 5% CO_2 for 6 h. Plates were then equilibrated at 25°C for 15 min before the introduction of Bio-Glo™ into each well. Plates were left 30 min at 25°C before luminescence reading on a PerkinElmer Victor 2030 plate reader.

Generation of mouse anti-P18FL antibodies. Six-week-old female BALB/cByJ mice (Charles River) were immunized with MBP-P18FL following 4 subcutaneous injections at Days 0, 14, 28 and 42 (25 µg MBP-P18FL/injection in combination with complete Freund adjuvant (CFA) at Day 0 and incomplete Freund adjuvant (IFA) at Days 14, 28 and 42). Blood samples were collected at Day -1 (pre-immune serum) and at Day 52 (immune serum). Mice immunization was performed by Biotem (Grenoble, France, ISO9001:2015; certificate FR0536014-1). Animal immunization was executed in strict accordance with good animal practices, following the EU animal welfare legislation and after approval of the INSERM and Biotem ethical committees.

Anti-CD20 BMFP-mediated opsonization of RAJI and EL4-huCD20 cells. RAJI or EL4-huCD20 target cells (2.5 x 10^5) were distributed in a 96-well plate pre-coated with PBS 1% BSA for 1 h at RT. To prevent non-specific binding, cells were incubated with PBS 1% BSA for 1 h at 4°C. Cells were then pelleted and resuspended in 100 µl of PBS 1% BSA containing 0.48 µM $scFv_{2H7}$-P18F3. Following 1 h incubation at 4°C, cells were washed three times with 200 µl PBS 1% BSA and resuspended in 100 µl of individual mouse serum (diluted from 1/10) in PBS 1%. After 1 h, cells were washed three times with 200 µl PBS 1% BSA and resuspended in 100 µl of PBS 1% BSA containing AffiniPure $F(ab')_2$ fragment goat anti-mouse IgG (H+L) PE-conjugated (1/100) (Jackson Immunoresearch). After 45 min, cells were washed three times with 200 µl PBS

and subjected to flow cytometry analysis in the presence of TO-PRO®-3 diluted 1/10,000 to discriminate live and dead cells.

***In vivo* tumor therapy.** Six-week-old female immunocompetent C57Bl/6 mice (Charles River) were immunized with MBP-P18FL by 3 subcutaneous injections at Days 0, 14 and 28 (25 µg MBP-P18FL/injection in combination with CFA at Day 0 and IFA at Days 14 and 28). Mice were then intravenously inoculated in the tail vein on Day 0 with 2.5 x 10^5 EL4-huCD20 cells per mouse (in 200 µL PBS, pH 7.4), 56 days (experiment 1, **Fig 6c**) or 10 days (experiment 1, **Fig 6d**) after the last immunization with MBP-P18FL. $ScFv_{2H7}$-P18F3 therapy was given as 4 intraperitoneal injections of 57 µg per mouse (in 200 µl PBS, pH 7.4) on Days 1, 4, 7 and 10. Another group of mice received 46 µg of $scFv_{2H7}$ (in 200 µl PBS, pH 7.4) according to the same injection schedules. Animals were followed daily for up to 120 days. Mice were euthanized as soon as one of the following clinical criteria appeared: presence of tumor on palpation, hindquarter paralysis, prostration, weight loss, hair bristling, abnormal abdominal swelling. Blood samples were collected 2 days before and 15 days after the start of the treatment. Animal experimentation was performed in compliance with guidelines from the European Union (EU guideline on animal experiments, European Directive #2010/63/ EU) and the national charter on ethics in animal experiments and was approved by the local Charles Darwin Ethics Committee in Animal Experiments, Paris, France (Authorization Number 01530.02).

Analysis of anti-$scFv_{2H7}$-P18F3 IgG subclasses. Ultra-high binding flat bottom microtiter 96-well plates (Immulon 4HBX) were coated overnight at 4°C with 100 µl of $scFv_{2H7}$-P18F3 at 1 µg/ml in PBS. Plates were then washed 3 times with 200 µl PBS and blocked for 1 h at RT with

100 µl of PBS 1% bovine serum albumin (BSA) (Sigma). After blocking removing solution, individual mouse sera (1/5) in PBS 1% BSA were added into the wells and incubated for 1 h at RT. Plates were then washed three times with PBS. One hundred microliters of goat anti-mouse IgG1, IgG2a, IgG2b or IgG3 Alkaline Phosphatase (AP)-conjugated (Jackson Immunoresearch) diluted 1/4,000 in PBS 1% BSA were added to each well and incubated for 45 min at RT. Plates were then washed three times with PBS and 100 µl of TMB (3,3',5,5'-tetramethylbenzidine) substrate (Biorad) were added per well. Absorbance was measured at 415 nm on an iMARK microplate absorbance reader (Biorad).

Antibodies. All antibodies used in the study are listed in **Supplementary Table 1**.

REPORTING SUMMARY

Further information on research design is available in the Nature Research Reporting Summary provided with the manuscript.

DATA AVAILABILITY

The data supporting the findings of this study are available within the manuscript and/or its supplementary materials. Any addition information could be provided upon request.

Figures

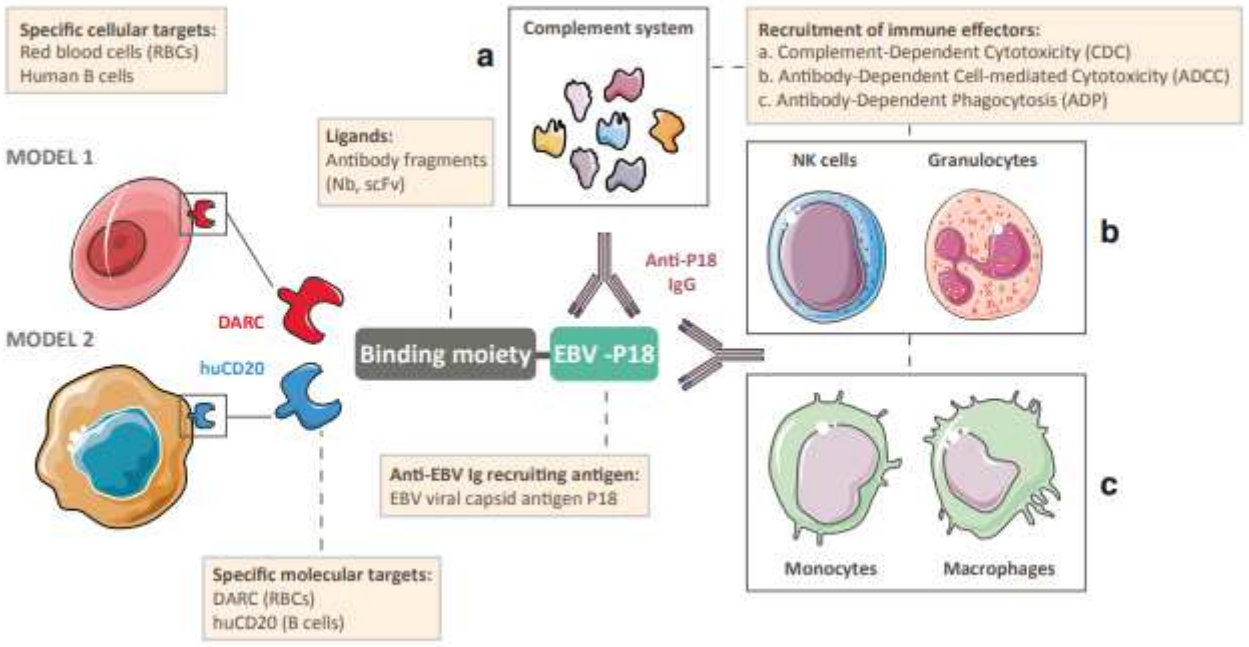

Figure 1

Conceptual modes of action of bi-modular fusion proteins (BMFPs). The EBV-P18 antigen is bound by circulating anti-EBV IgG present in the plasma of individuals chronically infected by EBV. Once fused to a binding moiety specifically directed to a molecule expressed by the targeted cells, P18 can serve as a recruiting agent for endogenous anti-P18 IgG and mediate their opsonization. The subsequent triggering of antibody-dependent effector mechanisms, i.e., complement activation via Fcγ binding to the complement component C1q (a) and/or ADCC and phagocytosis by immune cells expressing Fcγ receptors (b, c) ultimately leads to the elimination of the target cells. Target cells and relevant target molecules developed in the two models assessed in this study are depicted. Nb: Nanobody. ScFv: Single-chain Fragment variable. DARC: Duffy Antigen Receptor for Chemokines. huCD20: human Cluster of Differentiation 20. The art pieces used in the figure were obtained from Servier Medical Art by Servier, licensed under a Creative Commons Attribution 3.0 Unported License (https://smart.servier.com/) and modified.

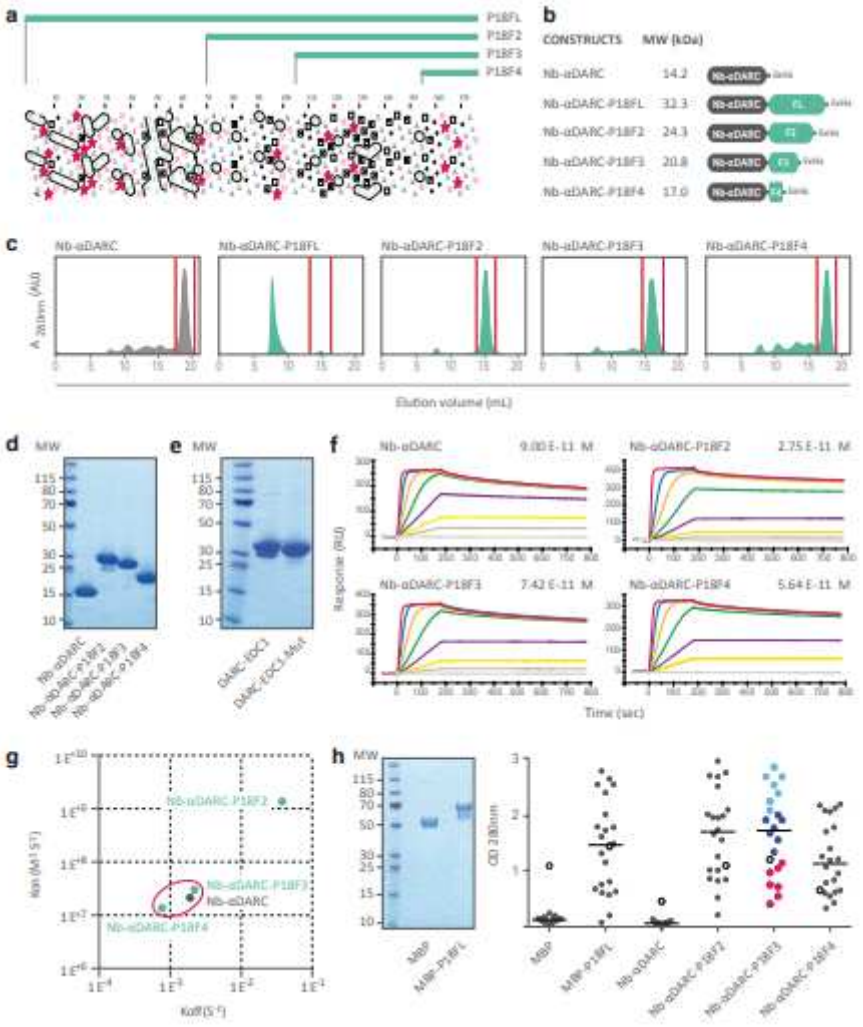

Figure 2

Engineering bi-modular fusion proteins (BMFPs) against DARC. (a) Hydrophobic cluster analysis plot of P18 (EBV strain B95-8). Strong hydrophobic amino acids are encircled, and their contours are joined, forming clusters. Analysis performed with HCA 1.0.2 (Ressource Parisienne en BioInformatique Structurale). Three P18-derived fragments (P18F2, P18F3, P18F4) have been designed with regard to their limited content in hydrophobic clusters. (b) Architecture of BMFPs comprising a nanobody (Nb) targeting the Duffy Antigen Receptor for Chemokines (DARC) and P18 fragments of different lengths. MW: Molecular weight. (c) Gel filtration profiles of Nb-αDARC and Nb-DARC-P18 BMFPs. For each sample, red bars delimit the protein of interest (POI) pick. AU: Arbitrary Units. (d) Purity of eluted POI was assessed by SDS-PAGE followed by Coomassie blue staining. (e) Following expression and purification, the purity of the GST fusion proteins DARC-ECD1 and DARC-ECD1-Mut (lacking the CA52 epitope) was assessed by SDS-PAGE followed by Coomassie blue staining. (f) Sensorgrams resulting from surface plasmon resonance analysis of the interactions between immobilized DARC and αDARC-P18 BMFPs. Nb-αDARC was included as a reference protein. Calculated KD values are displayed for each construct. RU: Response Units. M: molar. (g) RaPID plot resulting from SPR analysis of the interactions between DARC-EDC1 and the Nb-αDARC-P18 BMFPs. Calculated Kon and Koff values were plotted for each protein including Nb-αDARC. Both Nb-αDARC-P18F3 and Nb-αDARC-P18F4 cluster around Nb-αDARC within the red circle. (h)

Left panel. Following expression and purification, the purity of the MBP-P18FL fusion protein and of MBP alone was assessed by SDS-PAGE followed by Coomassie blue staining. Right panel. ELISA results of the binding of IgG present in plasma samples from 22 EBV+ individuals (1:100 dilution) to αDARC-P18 BMFPs. The full-length P18 polypeptide was included in the assay (MBP-P18FL). OD: Optical Density. MBP: Maltose-Binding Protein. Seven plasma samples displaying low, mild or high binding levels to Nb-αDARC-P18F3 (red, dark blue and light blue dots, respectively) were mixed together to obtained 3 different plasma pools (low, mild, high) to be used in further experiments (Fig. 3). The plasma sample recognizing both MBP (white dot) and Nb-αDARC alone (white dot) was excluded from pooling.

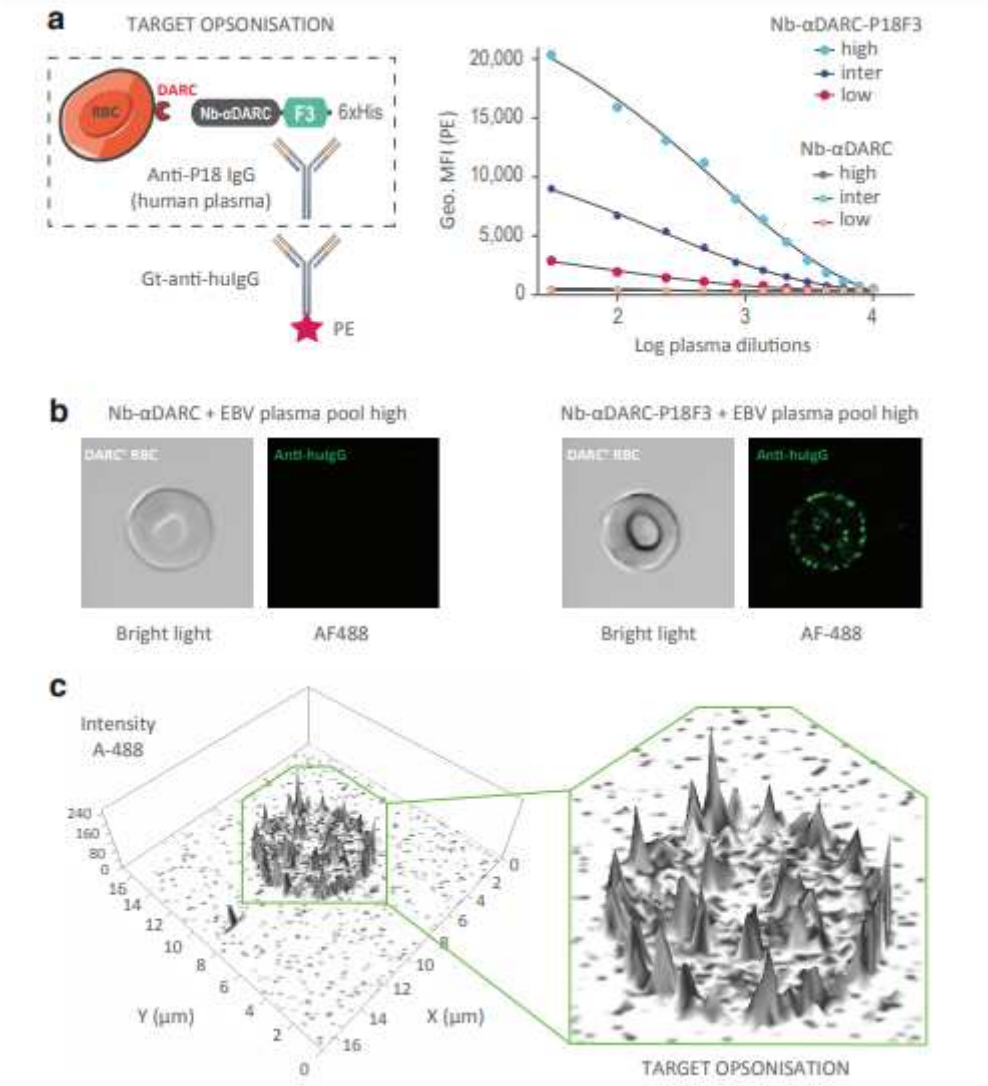

Figure 3

Nb-αDARC-P18F3 binds to native DARC and recruits anti EBV-human IgG (huIgG) to the RBC surface promoting target opsonisation. (a) The ability of Nb-αDARC-P18F3 to promote RBC opsonization by IgG present in the human plasma pools exhibiting different antibody titers against P18F3 was assessed by an indirect immunofluorescence assay and flow cytometry. Nb-αDARC and Nb-α DARC-P18F3 were used at a concentration that results in a similar binding to RBCs, 9.6 nM (Supplementary Fig 4). Membrane bound huIgG were detected using anti-huIgG antibodies conjugated to phycoerythrin (PE). Plotted data

represent the mean values of duplicates. (b) A qualitative analysis was performed by confocal microscopy to confirm that the signal resulting from huIgG detection was localized at the RBC surface. Upper panels. Confocal laser scanning microscopy images of huIgG distribution on the RBC membrane after incubation of RBCs with Nb-αDARC or Nb-α DARC-P18F3 in presence of plasma exhibiting a high antibody titer to P18F3. The binding of huIgG was revealed with goat Alexa Fluor-488-anti-huIgG antibodies (indicated as A-488). (c) 2.5D representation of the A-488 signal obtained when RBCs were incubated with Nb-α DARC-P18F3 in presence of plasma exhibiting a high antibody titer to P18F3. The right inset shows the enlarged 2.5D representation. Fluorescence is located at the RBC surface. Due to the biconcave shape of RBCs, membrane fluorescence located within the cell structure on the scanning microscopy images must not be mistakenly interpretated as cytosolic fluorescence. Confocal microscopy was performed with a Zeiss LSM700 microscope and images were analyzed with ZEN 2.0 software. AF-488: Alexa 488.

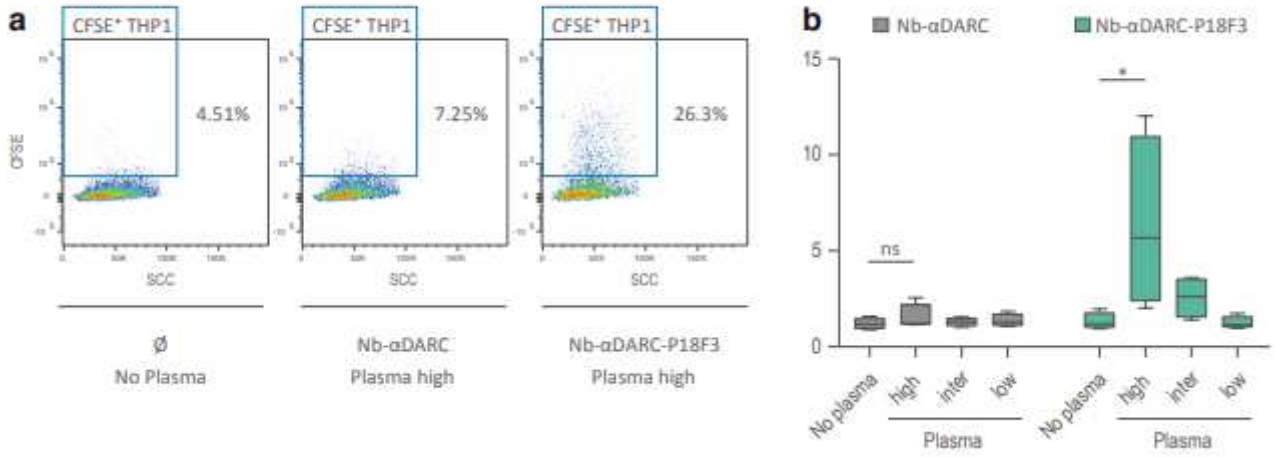

Figure 4

Nb-αDARC-P18F3-mediated huIgG RBC opsonization triggers erythrophagocytosis by macrophage-like THP1 cells. The ability of Nb-αDARC-P18F3 to promote RBC phagocytosis by THP1-derived macrophages was assessed in an erythrophagocytosis assay. CFSE-stained DARC+ RBCs were first incubated with Nb-αDARC or Nb-αDARC-P18F3 and with plasma pools exhibiting different antibody titers against P18F3. Following a 3h culture with THP1-derived macrophages, non-phagocytized RBCs were lysed and THP1 cells were then subjected to immunofluorescence analysis. (a) Representative data obtained from one experiment. A CFSE+ THP1 cell was regarded as a cell having phagocytized at least one RBC. Untreated cells (left panel) served as a reference for basal erythrophagocytosis by macrophage-like THP1-derived cells. Nb-αDARC-P18F3 treatment of RBCs in presence of plasma exhibiting a high antibody titer against P18 (indicated plasma high) led to a marked increase in the percentage of CFSE+ THP1 cells (right panel) as compared to Nb-αDARC-treated RBCs (middle panel). CFSE+ THP1 represents CFSE+ macrophage-like THP1-derived cells. SCC, Side SCatter. (b) Results obtained from 4 independent experiments are expressed as a fold increase (ordinate) in the percentage of CFSE+ macrophage-like THP1-derived cells incubated with RBCs coated with Nb-αDARC or Nb-αDARC-P18F3 and plasma pools exhibiting different

antibody titers against P18F3 (high, intermediate, low) compared to the percentage of CFSE+ cells incubated with untreated RBCs (i.e., no incubation with Nb-αDARC or Nb-αDARC-P18F3 and no plasma). Box plots include the mean horizontal line and interquartile range (box), whereas the whiskers represent the minimal and maximal values. Group comparison was performed using the non-parametric Mann-Whitney test. P-values < 0.05 were regarded as statistically significant (*). ns: non significant. Inter : intermediate.

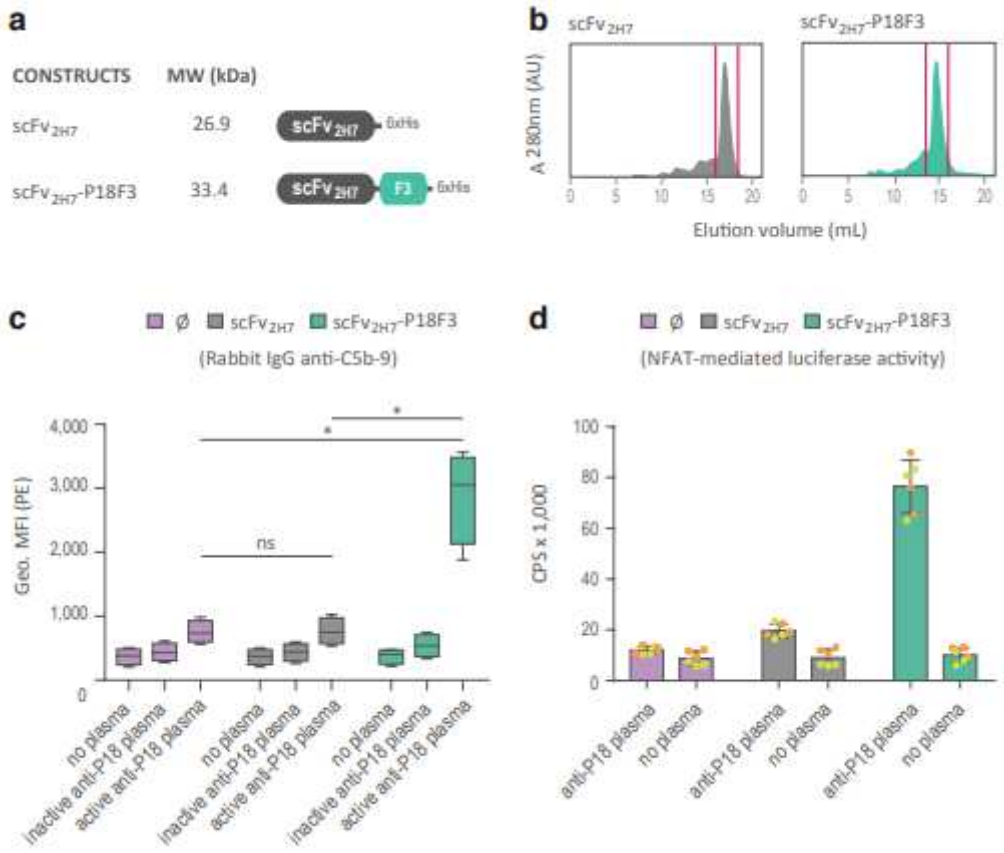

Figure 5

ScFv2H7-P18F3-mediated opsonization of Burkitt's Lymphoma cells induces activation of the antibody-dependent complement cascade and triggers FcγRIIIa-mediated activation of intracellular signaling pathways that leads to ADCC. (a) Architecture of BMFP (scFv2H7-P18F3) and of scFv2H7 targeting huCD20. MW: Molecular weight. (b) Gel filtration profiles of scFv2H7 and scFv2H7-P18F3. For each elution, red bars delimit the protein of interest (POI) pick. AU: Arbitrary Units. (c) The capability of scFv2H7-P18F3 to promote complement activation through the classical pathway (antibody-dependent) was assessed by monitoring the deposition of the membrane attack complex (MAC) C5b-9 at the surface of RAJI cells. RAJI cells were incubated with saturating concentration of scFv2H7 or scFv2H7-P18F3 and with a pool of human plasma exhibiting a high titer of anti-P18 antibodies. Ø: no scFv protein. Results obtained from 4 independent experiments are depicted. Box plots include the mean horizontal line and interquartile range (box), whereas the whiskers represent the minimal and maximal values. Group comparison was performed using the non-parametric Mann-Whitney test. P-values < 0.05 were regarded

as statistically significant (*). ns: non-statistically significant. (d) The capability of scFv2H7-P18F3 to promote the early events that lead to ADCC was assessed using a reporter assay. Activation of gene transcription through the NFAT pathway in competent effector Jurkat cells was quantified using a luciferase assay. RAJI cells were incubated with saturating concentration of scFv2H7 or scFv2H7-P18F3 and with a pool of human plasma exhibiting a high titer of anti-P18 antibodies and put in presence of Jurkat cells expressing human FcγRIIIa-V158 (ratio: 1:6) for 6 h. NFAT pathway activation was monitored by reading the luminescence of each plate well. CPS: counts per second. Ø: no scFv protein. Results obtained from 2 independent experiments performed in triplicates are depicted (exp.1 , exp.2). Boxes represent the mean values of the six measurements and the error bars depict the associated standard deviations.

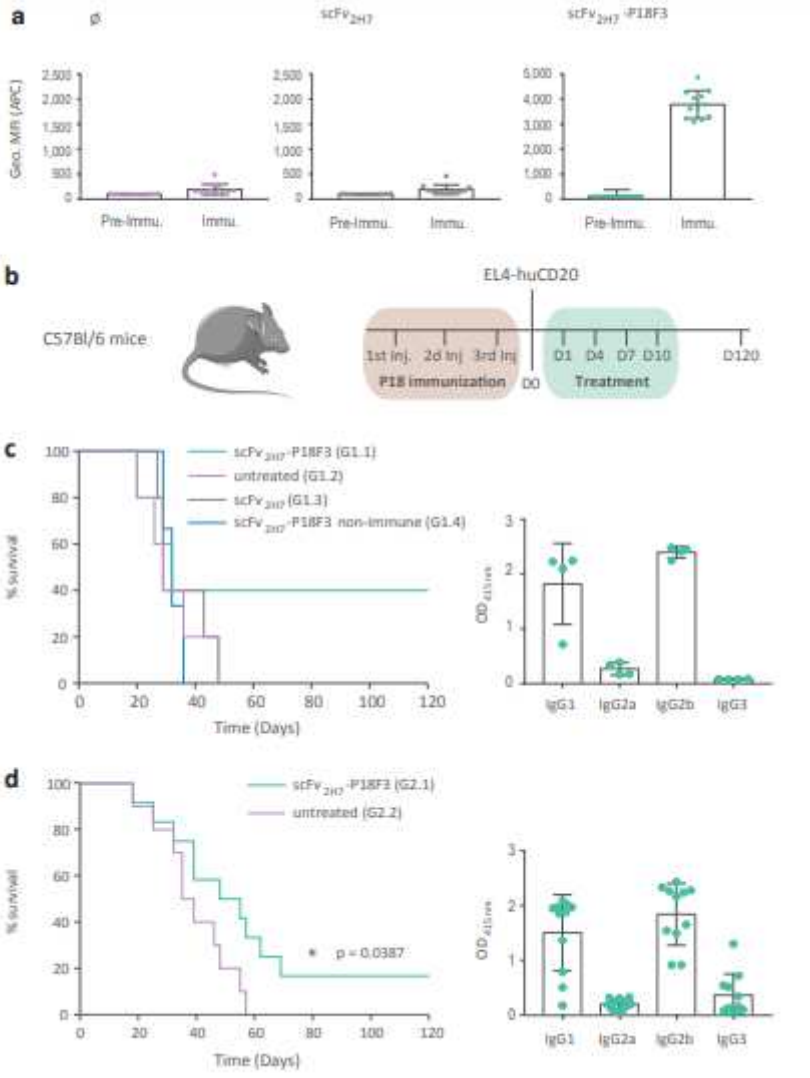

Figure 6

Treatment with scFv2H7-P18F3 reduces cancer progression in mice bearing EL4-huCD20 tumor cells. (a) Opsonization of scFv2H7- or scFv2H7-P18F3-coated EL4-huCD20 cells by IgG present in the individual sera (dilution 1/10) of 12 BALB/cByJ immunized with MBP-P18. Mouse IgG opsonization was assessed by labeling cells with donkey anti-mouse IgG (Fc) conjugated to allophycocyanin (APC) antibodies and

flow cytometry. Pre-Immu.: Pre-immune serum samples. Immu.: Immune serum samples. Ø: no scFv protein. Results obtained using EL4-WT cells are shown in Supplementary Fig. 11b. (b) The anti-tumor effect of ScFv2H7-P18F3 therapy was assessed in a mouse tumor model in two series of experiments. C57Bl/6 mice were pre-immunized with MBP-P18FL with four subcutaneous injections (25 µg MBP-P18-FL/injection). Mice were then injected with 2.5 x 105 EL4-huCD20 cells at Day 0 (D0) and received ScFv2H7-P18F3 therapy, consisting in 4 intraperitoneal injections at Days 1, 4, 7 and 10 (57 µg scFv2H7-P18F3/injection). Mice were followed-up for up to 120 days and were euthanized as soon as one of the following clinical criteria appeared: Presence of tumor on palpation, hindquarters paralysis, prostration, weight loss, hair bristling, abnormal abdominal swelling. (c) Left panel. Four groups (G) of 5 mice were differentially treated. Mice belonging to G1.1 and G.1.4 received scFv2H7-P18F3 therapy but mice from G.1.4 were not pre-immunized with MBP-P18FL (non-immune). Pre-immunized mice from G1.3 received scFv2H7 therapy. Right panel. Anti-P18F3 IgG subclasses were analyzed by ELISA from serum samples collected 2 days before EL4-huCD20 injection into G1.1 mice. OD: Optical Density. (d) Left panel. Two groups of mice were differentially treated. Mice belonging to G2.1 (n=12) received scFv2H7-P18F3 therapy whereas mice from G2.2 (n=11) received PBS. Comparison of survival curves was performed using a Log-rank (Mantel-cox) test. $\chi 2 = 4.275$. The P-value < 0.05 was considered as statistically significant (*). Right panel. Anti-P18F3 IgG subclasses were analyzed by ELISA from serum samples collected 2 days before EL4-huCD20 injection into G2.1 mice. The art pieces used in the figure are modified from Servier Medical Art by Servier, licensed under a Creative Commons Attribution 3.0 Unported License (https://smart.servier.com/).

Supplementary Files

This is a list of supplementary files associated with this preprint. Click to download.

- SUPPLEMENTARYFIGURESfinal.pdf